Available online at www.sciencedirect.com
ScienceDirect
Journal of Nuclear Materials 359 (2006) 59–68
journal of nuclear materials
www.elsevier.com/locate/jnucmat

Corrosion behavior and oxide properties of Zr–1.1 wt%Nb–0.05 wt%Cu alloy

Jeong-Yong Park *, Byung-Kwon Choi, Seung Jo Yoo, Yong Hwan Jeong

Advanced Core Materials Laboratory, Korea Atomic Energy Research Institute, 150 Deokjin-dong, Yuseong-gu, Daejeon 305-353, Republic of Korea

Received 20 March 2006; accepted 25 July 2006

Abstract

The corrosion behavior and oxide properties of Zr–1.1 wt%Nb–0.05 wt%Cu (ZrNbCu) and Zircaloy-4 have been investigated. The corrosion rate of the ZrNbCu alloy was much lower than that of the Zirclaoy-4 in the 360 °C water and 360 °C PWR-simulating loop condition without a neutron flux and it was increased with an increase of the final annealing temperature from 470 °C to 570 °C. TEM observations revealed that the precipitates in the ZrNbCu were β-Nb and ZrNb Fe-precipitate with β-Nb being more frequently observed and that the precipitates were more finely distributed in the ZrNbCu alloy. It was also observed that the oxides of the ZrNbCu and Zircaloy-4 consisted of two and seven layers, respectively, after 1000 days in the PWR-simulating loop condition and that the thickness of a fully-developed layer was higher in the ZrNbCu than in the Zircaloy-4. It was also found that the β-Nb in ZrNbCu was oxidized more slowly when compared to the $Zr(Fe,Cr)_2$ in Zirclaoy-4 when the precipitates in the oxide were observed by TEM. Cracks were observed in the vicinity of the oxidized $Zr(Fe,Cr)_2$, while no cracks were formed near β-Nb which had retained a metallic state. From the results obtained, it is suggested that the oxide formed on the ZrNbCu has a more protective nature against a corrosion when compared to that of the Zircaloy-4.

1. Introduction

The Zr fuel claddings in light water reactors are being challenged by several operational issues such as an extension of discharge burn-up, power uprating and a more corrosive coolant chemistry. A burn-up extension is desirable in the context of the economics of a reactor operation, but this is hard to realize without an improvement in the corrosion resistance of the Zr fuel claddings. Such a concern has promoted a great number of researches on Zr fuel cladding which has meant the development of advanced Zr alloys as a substitute for the Zircaloys [1–4].

In many previous results obtained from advanced Zr alloys [1–4], a Nb addition was proven to be very beneficial for increasing the corrosion resistance of the Zr alloys. However, the addition of Nb should be accompanied by an elaborate heat treatment because the corrosion resistance of Zr alloys has

* Corresponding author. Tel.: +82 42 868 8911; fax: +82 42 862 0432.
E-mail address: parkjy@kaeri.re.kr (J.-Y. Park).

0022-3115/$ - see front matter © 2006 Elsevier B.V. All rights reserved.
doi:10.1016/j.jnucmat.2006.07.017

been reported to be very sensitive to the Nb concentration as well as the heat treatment [5,6]. More recently, a Cu addition was reported to be effective for reducing the corrosion rate of Nb-containing Zr alloys in 360 °C water containing B and Li [7]. From a previous result by the authors [4], an advanced Zr alloy, Zr–1.1 wt%Nb–0.05 wt%Cu which was named HANA-6 showed a much better corrosion resistance when compared to the Zirclaoy-4 in various corrosion conditions.

However, the corrosion mechanism of Zr alloys has not really been established so far, even though a number of empirical relations between the corrosion behavior and the microstructures of an alloy and oxide have been reported by many researchers. Moreover, the corrosion behavior of the Nb-containing Zr alloys was not fully established by the previous results obtained for Zircaloy-4 suggesting that the corrosion mechanism of the Nb-containing Zr alloy was not the same as that of the Zirclaoy-4 [8].

This study aims at enhancing the understanding of the corrosion mechanism of Nb-containing Zr alloys. The corrosion behavior, microstructure and oxide properties of Zr–1.1 wt%Nb–0.05 wt%Cu have been investigated and correlated with each other to explore the reason why this alloy showed a better corrosion resistance than Zircaloy-4.

2. Experimental procedure

Nb-containing Zr alloy with a nominal composition of Zr–1.1 wt%Nb–0.05 wt%Cu (hereafter referred to as ZrNbCu) was used together with Zircaloy-4 in this study. The analyzed chemical compositions of the alloys are shown in Table 1. ZrNbCu was fabricated as a cladding tube with an outer diameter of 9.5 mm and a wall thickness of 0.57 mm while the Zircaloy-4 tube was used as-received. The final annealing for the manufactured ZrNbCu tube was applied at three different temperatures, i.e. 470 °C, 510 °C and 570 °C to assess the effect of the final annealing temperature on the corrosion behavior.

The microstructure of the alloys was observed by a transmission electron microscopy (TEM). The types of precipitates in the alloys were identified by analyzing the selected area diffraction pattern (SADP) and the chemical composition from the energy dispersive X-ray spectroscopy (EDS). The samples for the TEM observation were prepared by thinning the tube to a thickness less than 70 μm by using a solution of 10 vol.% HF, 30 vol.% H_2SO_4, 30 vol.% HNO_3 and 30 vol.% H_2O followed by a twin jet polishing with a solution of 10 vol.% $HClO_3$ and 90 vol.% C_2H_5OH.

Corrosion tests of the alloys were performed in a 360 °C water condition by using a static autoclave for 1020 days and in a 360 °C PWR-simulating loop condition without a neutron flux for 1000 days. Table 2 shows the detailed operating conditions of the PWR-simulating loop used in this study. The samples for the corrosion test were cut from the tube into segments with a length of 40 mm for ZrNbCu and 30 mm for Zircaloy-4 and then pickled in a solution of 10 vol.% HF, 30 vol.% H_2SO_4, 30 vol.% HNO_3 and 30 vol.% H_2O.

After the corrosion tests, a cross-section of the oxide was observed by a variety of methods such as a conventional optical microscopy (OM), transmitted light optical microscopy (TLOM), scanning electron microscopy (SEM) and TEM. The cross-section oxide sample for the TEM observation was prepared by mechanical thinning to a thickness of less than 20 μm followed by ion milling by using a Fishione Lamp 1010. Before the ion milling process, a mechanically thinned sample was also used for TLOM.

Nano-hardness of the oxide was measured as a function of the distance from the interface by using

Table 2
Operation condition of PWR-simulating loop used in this study

Parameter	Conditions
Temperature	360 °C
Pressure	18.5–18.8 MPa
Flow rate	3–4 l/h
[Li]/[B]	2.2 wppm/650 wppm
pH	6.8
Dissolved oxygen	<5 wppb
Conductivity	25 mS/cm

Table 1
Analyzed chemical compositions of the alloys used in this study (in wt%)

Alloy	Nb	Sn	Fe	Cr	Cu	O	C	Si	N	H (wppm)
ZrNbCu	1.12	<0.001	0.046	<0.01	0.08	0.132	0.010	0.010	<0.002	<3
Zircaloy-4	<0.001	1.34	0.21	0.11	0.0011	0.119	0.014	0.0084	0.0022	<8

a Nano Indentor XP. A nano-indentation was performed for a cross-section of the oxide at an interval of 300 nm in a direction perpendicular to the interface.

3. Results

3.1. Corrosion behavior

Fig. 1 shows the corrosion behavior of the ZrNbCu and Zircaloy-4 in 360 °C water for 1020 days. ZrNbCu showed a much lower corrosion rate than Zircaloy-4, irrespective of the final annealing temperature although the corrosion rate of ZrNbCu increased with an increase of the final annealing temperature. The weight gain of the 470 °C-annealed ZrNbCu which showed the lowest corrosion rate was less than 1/3 of that of the Zircaloy-4 corroded for the same duration. On the other hand, the corrosion rate of ZrNbCu in this study was found to be about half of that obtained for the Zr–1.0 wt%Nb in the authors' previous result [9]. This implies that the addition of Cu was very effective to reduce the corrosion rate of Zr–Nb binary alloy with about 1 wt%Nb in 360 °C water condition although it was taken into account that the chemical composition and the manufacturing process of the tube used in this study was further optimized when compared to the experimental alloys in the previous study [9].

Fig. 2 shows the corrosion behavior of the ZrNbCu and Zircaloy-4 in the PWR-simulating loop condition for 1000 days. ZrNbCu also showed a much lower corrosion rate than Zircaloy-4 in the PWR-simulating loop conditions. The corrosion rate of ZrNbCu was increased with an increase of the final annealing temperature in both conditions, but the increment of the corrosion rate with the final annealing temperature was relatively small in the PWR-simulating loop when compared to the 360 °C static water condition as shown in Fig. 3. All the alloys showed a lower corrosion rate in the PWR-simulating loop condition than in the 360 °C static water condition. This was caused by the fact that the dissolved oxygen concentration in the PWR-simulating loop was maintained below

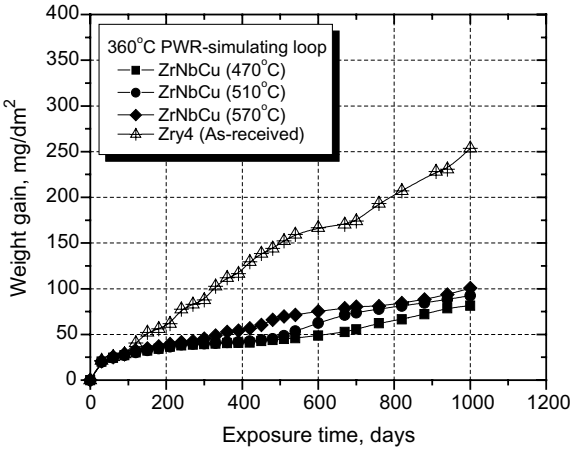

Fig. 2. Corrosion behavior of the ZrNbCu and Zircaloy-4 in the PWR-simulating loop condition. The temperatures in the parentheses indicate the final annealing temperatures for the ZrNbCu.

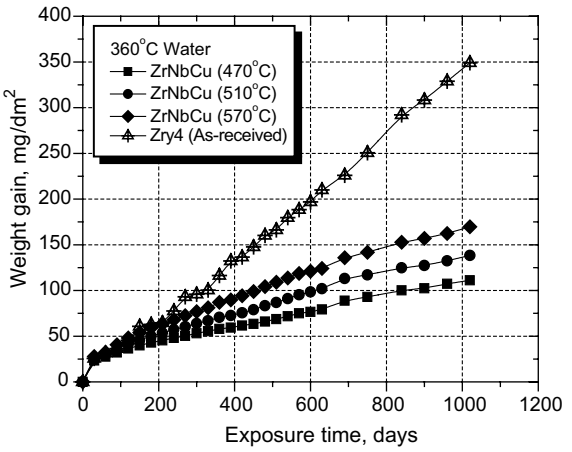

Fig. 1. Corrosion behavior of the ZrNbCu and Zircaloy-4 in the 360 °C water static autoclave. The temperatures in the parentheses indicate the final annealing temperatures for the ZrNbCu.

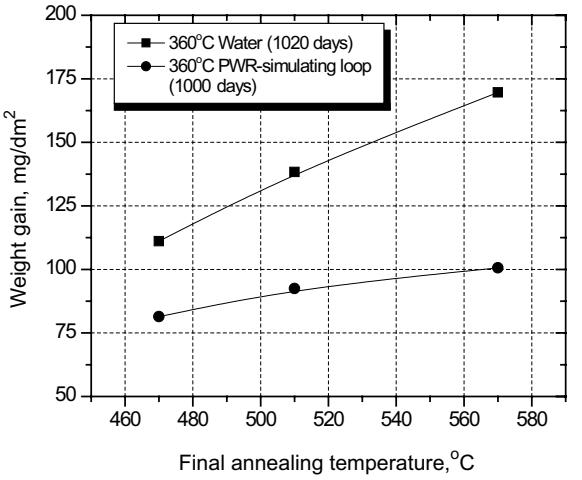

Fig. 3. Effect of the final annealing temperature on the corrosion behavior of the ZrNbCu in a 360 °C water and the PWR-simulating loop conditions.

5 wppb which is much lower than 8 wppm in the static autoclave. Therefore, it is suggested that the corrosion rate of the Zr alloys is highly dependant on the dissolved oxygen content even though the temperature is identical.

3.2. Precipitates in the alloys

Fig. 4 shows the microstructure of the ZrNbCu annealed at 470 °C, 510 °C and 570 °C. The microstructure of the ZrNbCu annealed at 470 °C consisted of entangled dislocations and recrystallized grains with a number of precipitates. When the final annealing temperature was increased, the entangled dislocations disappeared and the size of the recrystallized grain increased. It was found that the precipitates were more finely distributed in the ZrNbCu as compared to the Zircaloy-4.

The precipitates in ZrNbCu were identified by analyzing the SADP and the chemical compositions obtained form the EDS. Fig. 5 shows the precipitates found in the ZrNbCu annealed at 470 °C. The analysis on the precipitates revealed that the ZrNbCu annealed at 470 °C had two types of precipitates: β-Nb with a bcc crystal structure and ZrNbFe-precipitate with a fcc structure. β-Nb was more frequently observed when compared to ZrNbFe-precipitate in ZrNbCu alloy. Although Fe is not an alloying element of ZrNbCu alloy, a Fe impurity of about 500 wppm which is inevitable in

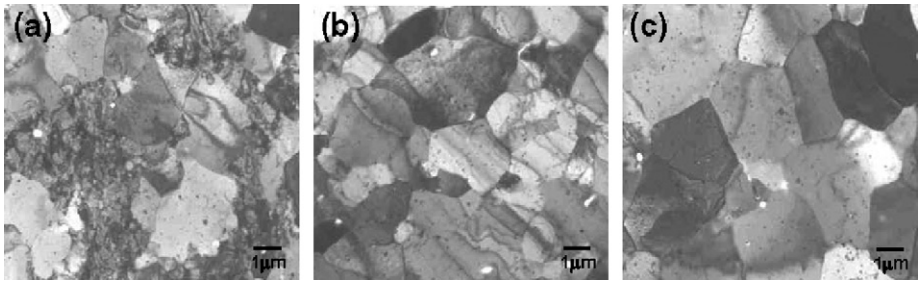

Fig. 4. Transmission electron micrographs of the ZrNbCu annealed at 470 °C, 510 °C and 570 °C.

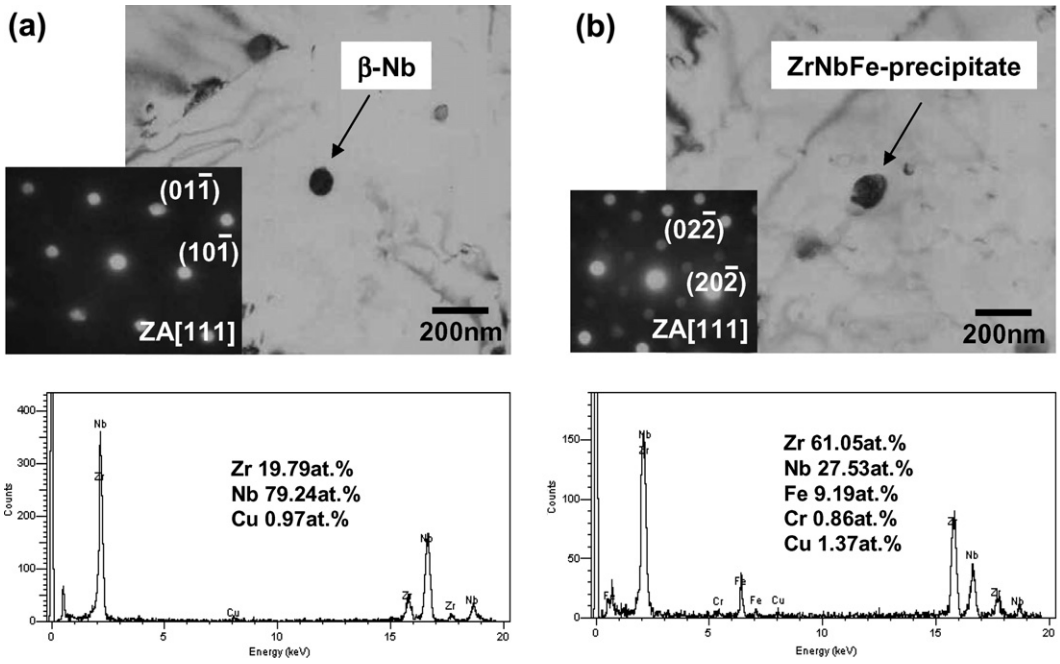

Fig. 5. TEM bright field image, selected area diffraction pattern and EDS spectrum with the analyzed chemical composition for the β-Nb and ZrNbFe-precipitate in ZrNbCu annealed at 470 °C.

a Zr sponge seems to be responsible for the formation of the Fe-containing precipitates. The Fe-containing precipitate with a fcc structure in ternary Zr–Nb–Fe system has been designated as $(Zr,Nb)_2Fe$ [10] or $(Zr,Nb)_4Fe_2$ [11] and was found to have approximately 30 at.% Fe [10,11]. In this study, however, the analyzed Fe content was about 9 at.% in the ZrNbFe-precipitate which had a fcc structure as shown in Fig. 5. This seems to be caused by the fact that the influence of Zr in the matrix was significant during the EDS analysis in this study.

Table 3 summarizes the characteristics of the precipitates in the ZrNbCu. The precipitate characteristics of ZrNbCu were not changed with an annealing temperature from 470 °C to 570 °C except that the particle size was increased with an increase of the final annealing temperature.

3.3. Oxide microstructure

Fig. 6 shows scanning electron micrographs of the cross-section of the oxide formed on the ZrNbCu annealed at 470 °C and Zircaloy-4 after a corrosion test for 1000 days in the PWR-simulating loop conditions. The interface was found to be more irregular in the Zirclaoy-4 showing a higher corrosion rate than ZrNbCu. This is in good agreement with a previous result [8]. On the other hand, the cross-section of the oxide had a rougher surface in the Zircaloy-4, even though the oxides of the two alloys were subjected to an identical polishing process with up to a 4000 grit abrasive paper. This result seems to be attributable to the fact that the oxide formed on Zircaloy-4 was more porous when compared to that of ZrNbCu.

Fig. 7 shows optical micrographs of the oxide cross-section of the ZrNbCu and Zicaloy-4. The reflected light optical micrographs showed that the interface of the ZrNbCu was smoother than that

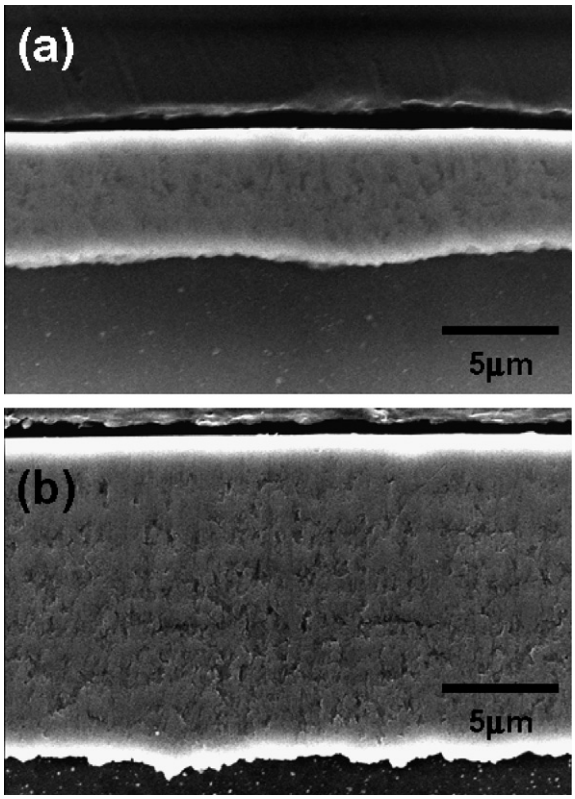

Fig. 6. Scanning electron micrographs on the cross-section of the oxide formed on the (a) ZrNbCu annealed at 470 °C for 8 h and (b) Zircaloy-4 after a corrosion test for 1000 days in the PWR-simulating loop conditions.

of the Zircaloy-4 as observed from the SEM image. Meanwhile, the transmitted light optical micrographs revealed that the oxide consisted of many layers, which was not observed from the reflected light optical micrographs. The layer structure in the transmitted light optical microscopy could have resulted from the fact that the transparency of the oxide is changed periodically, which is closely related to the changes of the grain morphology [12]. The transmitted light could have been scattered

Table 3
The characteristics of the precipitate in ZrNbCu

Final annealing temperature (°C)	Precipitate type	Frequency	Crystal structure	Chemical composition (at.%)	Average particle size (nm)
470	β-Nb	Major	BCC	19.8Zr–79.2Nb–1.0Cu	60
	ZrNbFe	Minor	FCC	61.0Zr–27.5Nb–9.2Fe–0.9Cr–1.4Cu	
510	β-Nb	Major	BCC	19.7Zr–79.3Nb–1.0Cu	70
	ZrNbFe	Minor	FCC	68.4Zr–23.5Nb–8.1Fe	
570	β-Nb	Major	BCC	20.7Zr–78.2Nb–1.1Cu	80
	ZrNbFe	Minor	FCC	57.2Zr–29.5Nb–12.1Fe–1.2Cu	

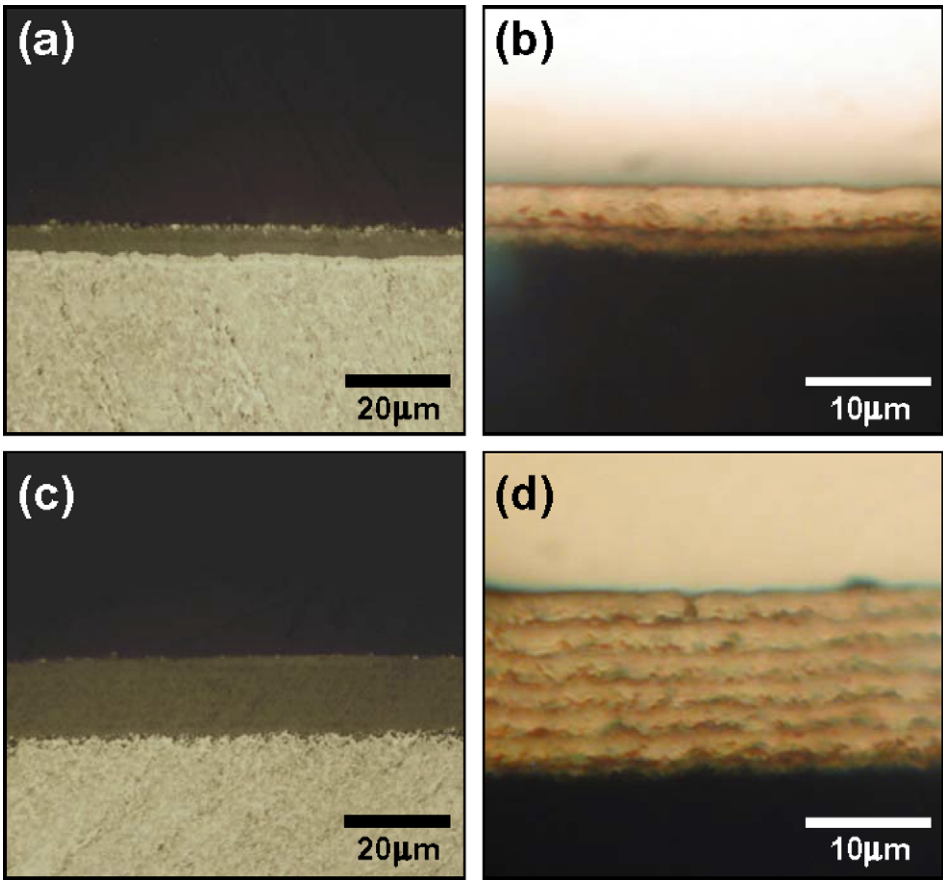

Fig. 7. (a) and (c) Reflected and (b) and (d) transmitted light optical micrographs on the cross-section of the oxide formed on the (a) and (b) ZrNbCu annealed at 470 °C for 8 h and (c) and (d) Zircaloy-4 after a corrosion test for 1000 days in the PWR-simulating loop conditions.

more in the smaller-sized equiaxed grains when compared to the columnar grains. This implies that the grain morphology is changed periodically when the oxide grows [13].

In the oxide of the ZrNbCu, two layers existed with different thicknesses. It was thought that the thicker layer was fully-developed whereas the thinner one adjacent to the interface was still developing. On the other hand, the oxide of Zirclaoy-4 was found to consist of six fully-developed layers and one developing layer. The characteristics of the oxide layer structures are summarized in Table 4. The most important factor related to the corrosion behavior of the alloys is thought to be the thickness of the fully-developed layer which was higher in the oxide of ZrNbCu, indicating that the oxide can become even thicker before an oxide transition in the ZrNbCu when compared to the Zircaloy-4.

Table 4
The characteristics of the layer structure observed in the oxide

	Total oxide thickness (μm)	No. of layer	Thickness of the fully-developed layer (μm)
ZrNbCu	4.3	2	2.9
Zircaloy-4	14.1	7	2.2

An oxide transition is usually accompanied by a cracking in an oxide [12] since the stress accumulated during an oxide growth has to be relaxed. Therefore, the oxide of ZrNbCu could withstand a higher stress before a transition or a stress accumulation in the oxide could be lower in the ZrNbCu when compared to Zircaloy-4. Although an exact explanation is not available at present, it is suggested that a resistance to a cracking is higher in the oxide of ZrNbCu.

3.4. Nano-hardness of the oxide

Nano-indentation test method is considered as a promising and appropriate technique for obtaining the local mechanical properties in an oxide to facilitate the analysis of the mechanical properties of an oxide from the context of a transition during an oxide growth. Fig. 8 shows the nano-hardness as a function of the position in the oxide formed on the ZrNbCu and the Zicaloy-4. In the case of Zircaloy-4, the nano-hardness values were considerably varied according to the position in the oxide from 5.6 GPa to 16.6 GPa. In the oxide of ZrNbCu, however, the nano-hardness ranged from 9.3 GPa to 12.2 GPa. The scattering range of the nano-hardness value was relatively small in the ZrNbCu when compared to Zricaloy-4. The scattering of the nano-hardness value seems to be attributable to the existence of defects such as cracks rather than the intrinsic properties of oxide indicating that the oxide of the Zirclaoy-4 was more porous than that of the ZrNbCu.

In this study, it was difficult to find any relationship between the nano-hardness variation and the layer structure shown in Fig. 7. However, it is noteworthy that the average nano-hardness is lower in the oxide of ZrNbCu. In general, a hardness value provides information on the resistance of materials to a plastic deformation: Harder materials are more susceptible to a cracking. It might imply that the softer oxide of ZrNbCu has a higher resistance to a cracking when compared to that of Zircaloy-4.

3.5. Precipitates incorporated into the oxide

It was well known that Zr alloys exhibit a different corrosion resistance depending on the characteristics of the precipitates. The precipitates are oxidized after they are incorporated into the oxide because the precipitates are usually more resistant to an oxidation when compared to the Zr matrix [14]. The grain morphology as well as the crystal structure of the oxide is significantly influenced by a delayed oxidation of the precipitate in the oxide. However, the influence of the precipitate on the oxide is different depending on the precipitate characteristics.

Fig. 9 shows the $Zr(Fe,Cr)_2$ precipitate located at about 500 nm away from the interface in the Zircaloy-4 corroded in the PWR-simulating loop for 1000 days. The $Zr(Fe,Cr)_2$ precipitate was found to be oxidized from the EDS results. We also observed that many cracks existed in the vicinity of the oxidized $Zr(Fe,Cr)_2$. On the other hand, the β-Nb located at a similar distance from the interface in the oxide of the ZrNbCu maintained a metallic state with no cracks nearby as shown in Fig. 10. It implies that $Zr(Fe,Cr)_2$ is more easily oxidized in the oxide of Zircaloy-4 when compared to the β-Nb in ZrNbCu. This result is in good agreement with a previous result [15]. Pecheur reported that unoxidized β-Nb was located in the oxide up to about 400 nm from the interface of Zr–1 wt%Nb while the $Zr(Fe,Cr)_2$ precipitate located at 350 nm from the interface of Zircaloy-4 was transformed to equiaxed nanocrystallites [15].

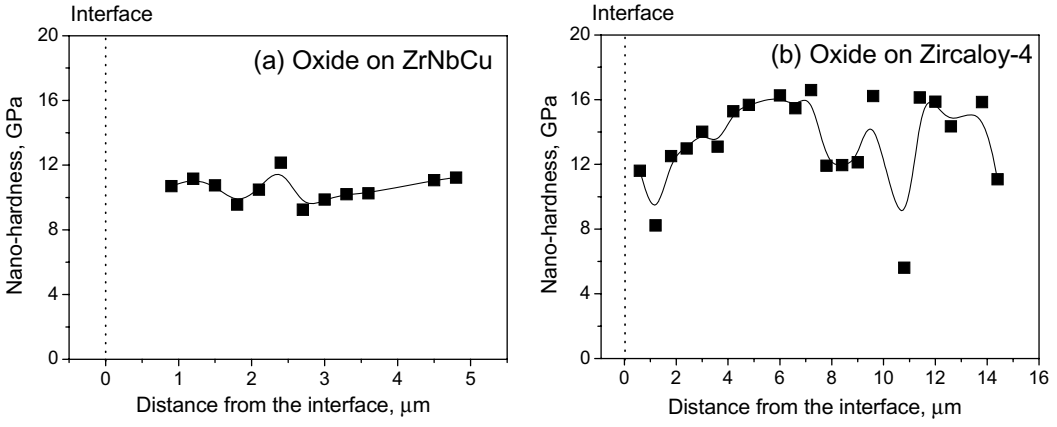

Fig. 8. Nano-hardness as a function of the distance from the interface in the oxide formed (a) ZrNbCu annealed at 470 °C for 8 h and (b) Zircaloy-4 after a corrosion test for 1000 days in the PWR-simulating loop condition.

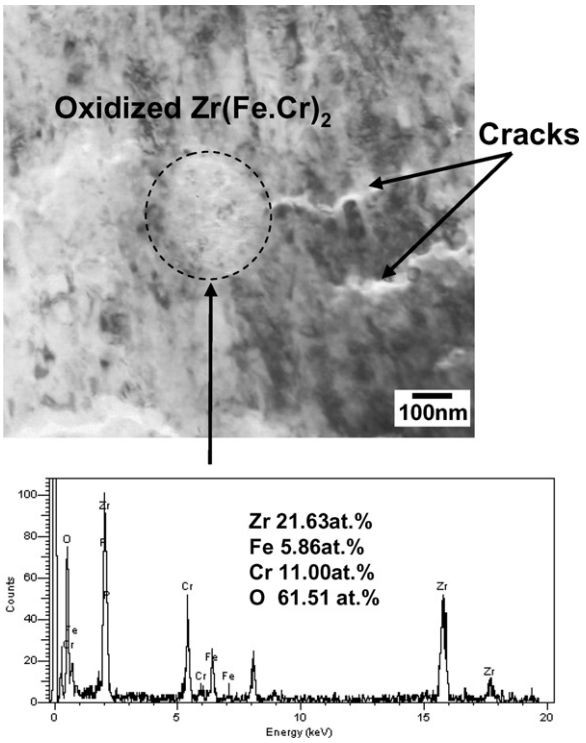

Fig. 9. $Zr(Fe,Cr)_2$ precipitate in the oxide formed on Zirclaoy-4 corroded to 1000 days in the PWR-simulating loop condition.

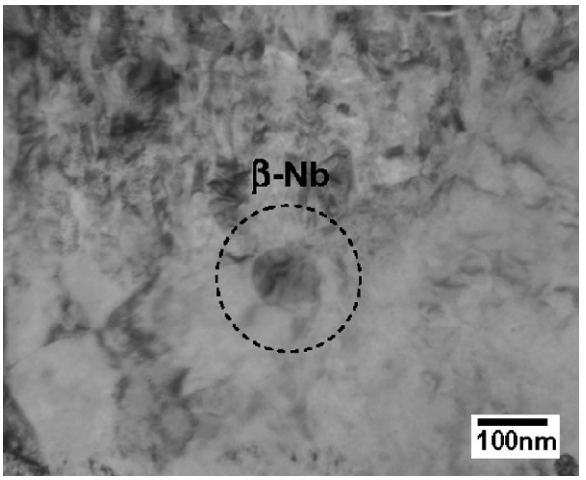

Fig. 10. β-Nb in the oxide formed on ZrNbCu corroded to 1000 days in the PWR-simulating loop condition.

4. Discussion

In this study, ZrNbCu showed a superior corrosion resistance to Zircaloy-4 in the 360 °C water (Fig. 1) and 360 °C PWR-simulating loop conditions (Fig. 2). In the Zr alloys used in this study, Fe and Cr existed in the form of precipitates whereas Sn was in the form of a solute element in the Zr matrix. On the other hand, Nb existed in the form of a solute element as well as precipitates. However, the Nb and Sn atoms in the form of solute elements have to be redistributed during the corrosion process [16] since the solubilities of Nb and Sn are very limited in ZrO_2. Takeda et al. reported that Sn was enriched at the boundaries of oxide crystallites [16]. It was also known that the high purity unalloyed Zr manufactured by van Arkel process could grow longer columnar grains during the oxidation process as compared to Zircaloy-4. This implies that the solute elements accumulated at the oxide/metal interface during the oxidation process could inhibit further columnar oxide growth and promote the nucleation of new columnar oxides. Therefore, the smaller amount of solute elements could be one of the reasons why the fully-developed layer was thicker in the oxide of ZrNbCu as compared to that of Zircaloy-4 as shown in Fig. 7.

On the other hand, it was confirmed from the nano-indentation test that the oxide on ZrNbCu was softer than that of Zircaloy-4 as shown in Fig. 8. In this study, however, the variation of the chemical composition, which can be correlated to the nano-hardness variation, was not measured in the oxide as well as at the interface. The hardness of the oxide is thought to be largely affected by the chemical composition rather than the grain morphology. Therefore, the difference in the hardness between the ZrNbCu and Zircaloy-4 originated from the differences in the distribution of alloying elements. The harder oxide on Zircaloy-4 could be attributed to the fact that the valence of Sn is lower when compared to Zr. The substitution of Sn with Zr in the ZrO_2 will increase the concentration of an oxygen vacancy while the addition of Nb whose valence is higher than Zr will reduce the concentration of an oxygen vacancy in ZrO_2. Oxygen vacancy will contribute to an increase of the hardness of the oxide as well as the corrosion rate. Moreover, a cracking could occur more easily in a harder oxide, which means that an oxide transition is more likely in the harder oxide of Zirclaoy-4 when compared to the softer oxide of ZrNbCu.

Meanwhile, the stable oxide types of Sn and Nb in the corrosion conditions used in this study are SnO and Nb_2O_5, respectively. Nb requires more oxygen when compared to Sn during an oxidation process. It implies that the volume fraction of the Sn oxide would be lower than the Nb oxide when

the same content of Sn and Nb is oxidized in ZrO_2. The solutionized Nb and Sn atoms are segregated into the grain boundary of the ZrO_2 and finally oxidized when the oxygen potential is sufficiently high enough for Nb or Sn to be oxidized. Such a delayed oxidation of the segregated elements might promote a cracking in the oxide, leading to an increase of the corrosion rate [16]. These phenomena would be more prominent in the Sn-containing alloys such as Zircaloy-4 because all the Sn existed in the form of a solid solution. However, this effect would be relatively small in the Nb-containing alloys like ZrNbCu since the solubility of Nb is lower when compared to Sn and a large amount of Nb existed in the form of a precipitate. This consideration is in good agreement with a previous result where the Zr–Nb alloys with an equilibrium Nb concentration in the matrix showed a lower corrosion rate than the supersaturated Nb-containing Zr alloys [17].

On the other hand, as mentioned before, a precipitate has been considered as the key parameter among the various metallurgical properties that influences most the corrosion resistance of Zr alloys. It was also found that the $Zr(Fe,Cr)_2$ precipitate was more likely to be oxidized in an oxide with some cracks propagated nearby when compared to β-Nb in ZrNbCu. It is not clear whether the cracks are attributable to an oxidation of the $Zr(Fe,Cr)_2$ since this might originate from the sample preparation process. However, the cracking seems to be caused by the fact that the additional stress build-up is higher when $Zr(Fe,Cr)_2$ is oxidized in the oxide. This would make the oxide more susceptible to a corrosion by enhancing the diffusion path of the oxidizing species in the oxide.

An oxide transition is usually accompanied by a cracking which has occurred in the case when the internal stress has reached a specific level. The oxidation of a precipitate exerts an additional stress on an oxide which already has an internal stress resulting from its growth. It implies that an additional stress build-up by an oxidation of a precipitate promotes an oxide transition. However, such an effect is considerably different depending on the precipitate morphology. It is thought that the distribution of an additional stress build-up by an oxidation of the precipitates is more homogenous in the case of ZrNbCu where the β-Nb was found to be finely distributed. Moreover, since the β-Nb in ZrNbCu was oxidized more slowly when compared to $Zr(Fe,Cr)_2$ in Zircaloy-4, an oxide transition would be delayed more in the ZrNbCu. This can be considered as the main reason why ZrNbCu showed a much better corrosion resistance than Zirclaoy-4.

This consideration can also provide a satisfactory explanation to the reason why a final annealing at a lower temperature is beneficial for the corrosion resistance of ZrNbCu. The beneficial effect of β-Nb would be enhanced when the particle size is reduced and the distribution is finer by a low temperature annealing because the stress induced by the oxidation of β-Nb will be more homogeneous and the oxide can grow to a greater thickness before a transition. Although the corrosion is controlled by a diffusion of the oxidizing species through the oxide both in the ZrNbCu and the Zircaloy-4, it is suggested that the oxide properties controlling the diffusion have a more protective nature in the ZrNbCu on the basis of the results obtained in this study.

5. Conclusions

The corrosion behavior and oxide properties of Zr–1.1 wt%Nb–0.05 wt%Cu (ZrNbCu) and Zircaloy-4 have been investigated. The corrosion rate of the ZrNbCu alloy was much lower than that of the Zirclaoy-4 in the 360 °C water and 360 °C PWR-simulating loop conditions without a neutron flux and it was increased with an increase of the final annealing temperature from 470 °C to 570 °C. TEM observations revealed that the precipitates in the ZrNbCu were β-Nb and ZrNbFe-precipitate with β-Nb being more frequently observed and that the precipitates were more finely distributed in the ZrNbCu alloy. It was also observed that the oxides of the ZrNbCu and Zircaloy-4 consisted of two and seven layers, respectively, after 1000 days in the PWR-simulating loop condition and that the thickness of a fully-developed layer was higher in the ZrNbCu than in the Zircaloy-4. Also it was found that the β-Nb in ZrNbCu was oxidized more slowly when compared to the $Zr(Fe,Cr)_2$ in Zirclaoy-4 when the precipitates in the oxide were observed by TEM. Cracks were observed in the vicinity of the oxidized $Zr(Fe,Cr)_2$, while no cracks were formed near β-Nb which had maintained a metallic state. From the results obtained, it is suggested that the oxide formed on the ZrNbCu has a more protective nature against a corrosion when compared to that of the Zircaloy-4.

Acknowledgement

This study was supported by KOSEF and MOST, Korean government, through its National Nuclear Technology Program.

References

[1] G.P. Sabol, G.R. Kilp, M.G. Balfour, E. Roberts, ASTM STP 1023 (1989) 227.
[2] J.-P. Mardon, D. Charquet, J. Senevat, ASTM STP 1354 (2000) 505.
[3] K. Yamate, A. Oe, M. Hayashi, T. Okamoto, H. Anada, S. Hagi, Proc. of the 1997 International Topical Meeting on LWR Fuel Performance (1997) 318.
[4] J.Y. Park, B.K. Choi, Y.H. Jeong, K.T. Kim, Y.H. Jung, Proc. of 2005 Water Reactor Fuel Performance Meeting (2005) 188.
[5] H.G. Kim, Y.H. Jeong, T.H. Kim, J. Nucl. Mater. 326 (2004) 125.
[6] Y.H. Jeong, K.O. Lee, H.G. Kim, J. Nucl. Mater. 302 (2002) 9.
[7] J.Y. Park, B.K. Choi, Y.H. Jeong, Y.H. Jung, J. Nucl. Mater. 340 (2005) 237.
[8] P. Bossis, J. Thomazet, F. Lefebvre, ASTM STP 1423 (2002) 190.
[9] A. Yilmazbayhan, A.T. Motta, H.G. Kim, Y.H. Jeong, J.Y. Park, R.J. Comstock, B. Lai, Z. Cai, in: Proc. of 12th Int. Conf. on Environmental Degradation of Materials in Nuclear Systems-Water Reactors, Salt Lake City, UT, USA, August 14–18, 2005.
[10] M.S. Granovsky, M. Canay, E. Lena, D. Arias, J. Nucl. Mater. 302 (2002) 1.
[11] P. Baberis, D. Charquet, V. Rebeyrolle, J. Nucl. Mater. 326 (2004) 163.
[12] A.T. Motta, A. Yilmazbayhan, R.J. Comstock, J.M. Partezana, G.P. Sabol, B. Lai, Z. Cai, J. ASTM Int. 2 (2005).
[13] A. Yilmazbayhan, E. Breval, A.T. Motta, R.J. Comstock, J. Nucl. Mater. 349 (2006) 265.
[14] D. Pecheur, F. Lefebvre, A.T. Motta, C. Lemaignan, J. Wadier, J. Nucl. Mater. 189 (1992) 318.
[15] D. Pecheur, J. Nucl. Mater. 278 (2000) 195.
[16] K. Takeda, H. Anada, ASTM STP 1354 (2000) 592.
[17] Y.H. Jeong, H.G. Kim, T.H. Kim, J. Nucl. Mater. 317 (2003) 1.